Development of a Pseudo Phased Array Technique using EMATs for DM Weld Testing

Adam C. Cobb[1,a)], Jay L. Fisher[1], Nobuyuki Shiokawa[2], Toshiaki Hamano[2], Ryoichi Horikoshi[2], and Nobukazu Ido[2]

[1]Southwest Research Institute
Sensor Systems and Nondestructive Technology Department
6220 Culebra Road
San Antonio TX 78238-5166 USA

[2]IHI Corporation
Nuclear Power Operations
Yokohama Engineering Center
1, Shin-Nakahara-cho, Isogo-ku
Yokohama 235-8501 Japan
Quality Control Group

[a)]Corresponding author: adam.cobb@swri.org

Abstract. Ultrasonic inspection of dissimilar metal (DM) welds in piping with cast austenitic stainless steel (CASS) has been an area ongoing research for many years given its prevalence in the petrochemical and nuclear industries. A typical inspection strategy for pipe welds is to use an ultrasonic phased array system to scan the weld from a sensor located on the outer surface of the pipe. These inspection systems generally refract either longitudinal or shear vertical (SV) waves at varying angles to inspect the weld radially. In DM welds, however, the welding process can produce a columnar grain structure in the CASS material in a specific orientation. This columnar grain structure can skew ultrasonic waves away from their intended path, especially for SV and longitudinal wave modes. Studies have shown that inspection using the shear horizontal (SH) wave mode significantly reduces the effect of skewing. Electromagnetic acoustic transducers (EMATs) are known to be effective for producing SH waves in field settings. This paper presents an inspection strategy that seeks to reproduce the scanning and imaging capabilities of a commercial phase array system using EMATs. A custom-built EMAT was used to collect data at multiple propagation angles, and a processing strategy known as the synthetic aperture focusing technique (SAFT) was used to combine the data to produce an image. Results are shown using this pseudo phased array technique to inspect samples with a DM weld and artificial defects, demonstrating the potential of this approach in a laboratory setting. Recommendations for future work to transition the technique to the field are also provided.

INTRODUCTION

Cast austenitic stainless steel (CASS) is used in the nuclear power industries, most notably in reactor coolant piping systems of pressurized water reactors (PWRs), because of its superior resistance to corrosion [1, 2]. Operational experience, however, has shown that when primary coolant water is present, these materials are susceptible to primary water stress corrosion cracking (PWSCC) [3]. Given this cracking concern, there is a need to develop reliable inspection techniques for these materials, particularly of the welds. Historically, ultrasonic inspection of austenitic welds was considered to be impractical because of the metallurgy of the material: grains are elongated and large compared to those found in ferritic steel, resulting in a high degree of acoustic anisotropy, beam distortion, and scattering [4]. Moreover, these elongated grains are often organized in columnar structures near

41st Annual Review of Progress in Quantitative Nondestructive Evaluation
AIP Conf. Proc. 1650, 1015-1022 (2015); doi: 10.1063/1.4914709

welds, which can result in the elastic waves being skewed in an unexpected direction. Beam skewing is particularly evident when using vertically polarized shear (SV) elastic waves, as shown in Fig. 1.

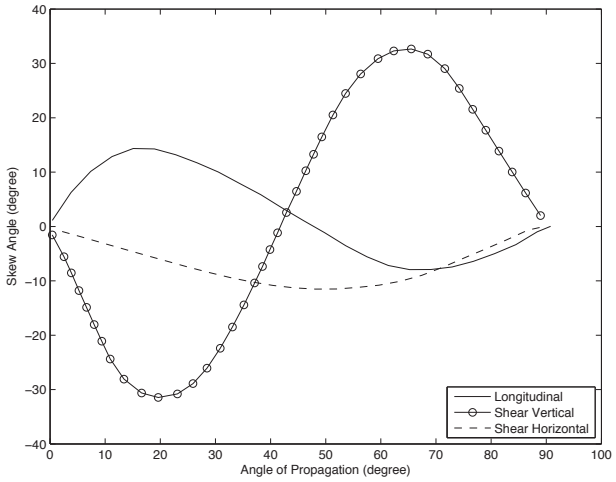

FIGURE 1. Relationship between skew and propagation angles relative to columnar direction of austenitic grains [1].

In recent years, inspection systems using phased array technology are becoming increasingly common for the inspection of welds in ferritic steel pipelines. These systems typically employ transducers in the frequency range of 2 to 4 MHz and utilize 16 or more elements to steer the sound within the base material to inspect the weld [5]. Additionally, SV wave mode transducers are typically employed for ferritic weld inspection. For the reasons discussed above, ferritic steel phased array system setups (2-4 MHz, SV wave mode) are not practical for inspection of austenitic steel welds. In an effort to overcome the metallurgical issues, researchers have shown that by lowering the frequency (1.5 MHz and below) to reduce scatter and attenuation, and by using specialized longitudinal (L) wave mode transducers to reduce beam skew, phased array inspection of austenitic welds is possible [6, 7]. Additionally, the use of physically larger transducers helps overcome the effect of beam skew as it gives a larger area for the reception of the bulk wave, but this can be problematic because of access constraints. Also, the use of L waves for inspection introduces additional concerns in the form of mode conversion from the boundaries, which complicates signal analysis. Thus, while phased array inspection of austenitic welds is possible with a specialized setup, there is potentially room for improvement in the approach to produce better inspection results.

Looking again at Fig. 1, it is clear that while L wave mode inspection provides an improvement over SV wave mode inspections, the best wave mode choice for inspection of austenitic welds is horizontally polarized shear (SH) waves; SH waves have the minimum theoretical beam skew and there is little concern for mode conversion at the boundaries. This wave mode, however, is more difficult to generate than L and SV wave modes using piezoelectric-based transducers, such as those associated with commercially available phased array systems. Electromagnetic acoustic transducers (EMATs), which function using the Lorentz effect and/or magnetostriction, are a practical alterative to piezoelectric transducers for generating and receiving SH waves for ultrasonic testing [8]. Additionally, because generation and reception mechanisms involve electromagnetic coupling from the transducer to the material itself, there is no need for liquid couplants that are required for piezoelectric-based transducers.

Given the advantages associated with SH waves, the concept of replicating the phased array functionality with EMATs has been investigated by other researchers [1, 9]. These systems function similarly to the piezoelectric-based phased array systems, utilizing custom systems and transducers that have up to 8 channels for generation and reception of the ultrasonic waves. These systems have been successfully demonstrated on realistic damage in mockups of nuclear power plant structures. The disadvantage of this approach is simply that specialized hardware (i.e., the acquisition system and transducer) is required, which may slow adoption of the technique.

The purpose of this work was to explore whether performance similar to what is possible using the commercially available phased array systems, both piezoelectric and EMAT-based, is achievable using more traditional EMAT sensors and systems. The approach was to build a single channel EMAT and process the waveforms collected using a signal processing technique known as synthetic aperture focusing technique (SAFT) to replicate the imaging and

inspecting capabilities of phased array systems without the use of specialized hardware. Additionally, SAFT allows the use of relatively smaller probes that can more easily match the geometry of the part under test while still allowing the focusing capability associated with larger probes. This pseudo phased array approach was tested using a dissimilar metal (DM) weld mockup that combined CASS, ferritic steel and Inconel.

TRANSDUCER DESIGN AND FABRICATION

The goal of this effort was to utilize a conventional EMAT design to replicate the functionality of a phased array system and inspect using the SH wave mode; this EMAT was connected to a single channel acquisition system suitable for working with EMATs. As such, the EMAT design must be able to generate and receive SH wave modes and provide some mechanism to steer the sound without requiring multiple transmit and receive channels.

Given these requirements, the specific type of EMAT pursued for this effort was a periodic permanent magnet (PPM) EMAT [8]. A PPM EMAT gets its name from an array of permanent magnets used in its construction, as shown in Fig. 2, where the magnets have a very specific orientation relative to one another that is repeated periodically. An RF coil is located between the magnet array and the part to be inspected. This EMAT generates sound using the Lorentz force effect, so it should be suitable for working with a wide variety of conductive materials. The advantage of this EMAT type is that the primary radiation direction of the SH wave is function of magnet array spacing period (D) and the operating frequency (f), given by the equation below

$$\sin\theta = v / fD \,, \tag{1}$$

where v is the shear wave speed and θ is the primary radiation angle. Thus for a given EMAT where D is fixed, the radiation angle can be changed by adjusting the operating frequency to steer the sound in the material. The obvious implication of this approach for steering, however, is that the data is collected at multiple frequencies to inspect over a range of angles, which is different from traditional phased array operation.

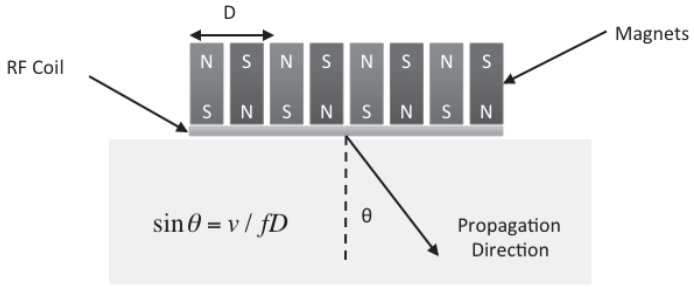

FIGURE 2. Side-view of a PPM EMAT.

For this effort, it was decided to pursue a low-frequency EMAT design to reduce the effect of the elongated grain size. For a PPM EMAT, the operating frequency to generate a given SH wave at a specific propagation angle is determined by the magnet spacing, D. Of the commercially available magnets (i.e., not custom magnets), the magnet thicknesses are typically available in 3.2 mm (0.125 inch) increments. The two thinnest available magnets are 3.2 mm and 6.4 mm, which correspond to operating frequencies of approximately 700 kHz and 350 kHz for generating a 45° SH wave in carbon steel (assumming 3.2 mm/μs velocity). Prior studies have shown that a lower test frequency improves the results, so it was decided to utilize the 6.4 mm thick magnets [7]. Although magnets with thicknesses greater than 9 mm are available, the test frequencies fall below 250 kHz for generating a 45° SH wave, and the system used during this study is not efficient at that low of a frequency.

Following definition of the magnet thickness, the PPM EMAT itself was fabricated. Two magnet arrays were constructed, each using eight magnets that were 25.4 mm by 12.7 mm by 6.4 mm. Each array had two columns of four magnets arranged as shown in Fig. 2, for a final array size of 25.4 mm by 25.4 mm by 25.4 mm. Two magnet arrays are necessary to allow for a pitch-catch mode of operation for the sensor, in which one array is used for transmit and the other is used for receive. Two racetrack-style EMAT coils were designed and manufactured as flexible printed circuit boards to serve as the RF coils. Finally, a mechanical housing was machined from aluminum (shown in Fig. 3) to protect the sensor from electromagnetic interference (EMI) as well as position the magnet arrays relative to one another. As can be seen, the two magnet arrays and RF coils (shown in the right-side photograph)

were angled toward one another slightly to maximize the signal return from a reflector approximately 140 mm from the sensor.

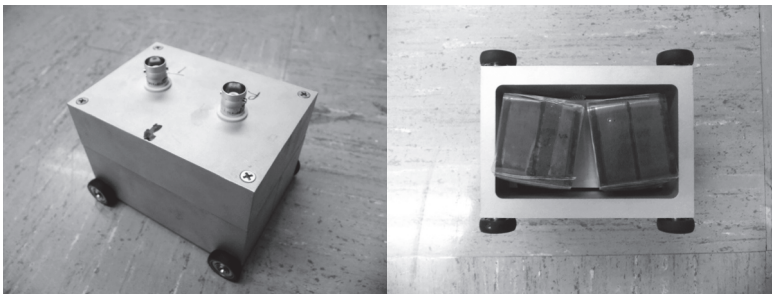

FIGURE 3. Photographs of the EMAT housing, showing the top (left) and bottom (right) of the completed transducer. The final EMAT was 88.9 mm wide by 63.5 mm long and 58.4 mm tall.

DATA COLLECTION STRATEGY

The motivating structure for this effort was inspection of a DM weld with Inconel buttering; this type of weld exists in many PWR nuclear power plants. The structure chosen for this project has an outer diameter (OD) of 1 m and a wall thickness of approximately 140 mm. The pipeline materials are CASS on one side of the weld and ferritic steel on the other side. While testing on this structure was not performed on this effort, it is instructive to consider the anticipated data collection approach.

The inspection concept is to scan the transducer around the circumference of the structure, pausing at regular intervals for data collection. The specific scan pattern anticipated is a raster scan, meaning that data will be collected both at a regular interval in the circumferential direction as well as at a regular interval axially along the pipe. The axial position for the transducer that is closest to the weld will be when the near edge of the transducer housing is in line with the visible edge of the base metal prior to the DM weld. At each location, data will be collected at multiple frequencies and thus multiple propagation angles. Table 1 summarizes the inspection frequencies for the data collection process suitable for the transducer designed on this effort.

TABLE 1. Inspection frequency and propagation angles for future field testing and mockup evaluations (assuming carbon steel).

Test Frequency	Propagation Angle
280 kHz	64.4°
300 kHz	58.0°
330 kHz	50.5°
350 kHz	46.6°
390 kHz	40.7°

In prior efforts, the authors have typically used a data collection interval less than the ultrasonic wavelength. From the above table and assuming a shear wave speed of 3.2 mm/microsecond, the ultrasonic wavelength ranges from 8.2 mm to 11.4 mm. Based on these values, it was decided to use an axial and circumferential data collection interval of 6.35 mm. Data will be collected completely around the circumference of the structure, which results in approximately 500 circumferential increments. It was decided to collect data in fifteen increments axially away from the weld, where this large number of increments was chosen to ensure that at the furthest position, no data collected at any inspection frequency would be able to inspect the weld; in other words, the furthest waveforms collected will serve as "baseline" waveforms.

This inspection procedure was validated using mockup specimens, shown in Fig. 4. The mockup was made by first welding ferritic and CASS steel pipes with Inconel buttering that were 1 m in diameter with wall thicknesses of approximately 140 mm. The welding process approximated typical fabrication methods. A section was then cut from pipe, resulting in a mockup that is 640 mm in length and 136 mm wide. A series of side-drilled holes were

added to the mockup as shown in the figure, where three are located in the DM weld and three are located in the CASS. The above data collection procedure was used to collect the data on the mockup with one modification; because of the narrow specimen width, it was not practical to scan the sensor in the circumferential direction so data was collected only in the axial direction. Also, the data was collected only on the carbon steel portion of the mockup. This decision was made for two reasons. First, the CASS portion of the mockup had additional side-drilled holes that would likely affect the inspection results when examining the DM weld. Second, CASS is far less conductive than ferritic steel and therefore produces much smaller signals with the EMAT sensor. Since this was a proof-of-concept demonstration, the simpler inspection originating on the ferritic portion of the mockup was justified.

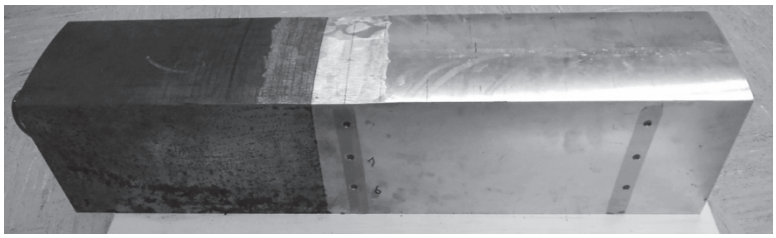

FIGURE 4. Mockup specimen used to verify the inspection approach.

DATA ANALYSIS STRATEGY

In previous efforts, the authors have implemented a signal processing strategy known as SAFT for a variety of nondestructive evaluation (NDE) inspection applications using data collected using a single sensor at multiple locations [10,11]. The concept is that the response from a flaw can be observed from a sensor even as the sensor is moved from one location to another. This is because the beams from the different transducer locations overlap and therefore provide redundant coverage of the structure. Based on the understanding of the beam-spread function, the SAFT processing algorithm exploits this redundancy to better characterize and localize any damage.

As an overview of the SAFT algorithm, the concept is to divide the structure into a Cartesian grid of locations. For the data collected during this effort, the *x* axis is along the axial length of the mockup specimen and the *y* axis is normal to the test specimen surface; as previously discussed, the final implementation of this technique in the field will involve circumferential scanning of the sensor that was not possible using the mockups available. For each (*x,y*) location, the beam forming response is given by

$$A^{x,y} = \sum_{p}\sum_{n} w_p^{x,y}(n)\, s_p(n) \tag{2}$$

where *p* denotes the sensor position, *n* denotes the waveform sample, $w_p^{x,y}(n)$ is a weighting function for position *p* and location (*x,y*), and $s_p(n)$ is the waveform recorded at position *p*. This algorithm computes the contribution from every sensor for each (*x,y*) location, resulting in a intensity image that allows for flaw identification.

The weighting function for each sensor position and location is computed using the angle $\theta_p^{x,y}$ and propagation distance $d_p^{x,y}$ between the sensor at position *p* and location (*x,y*). For this effort, the weighting function was given as

$$w_p^{x,y}(n) = a_p^{x,y}(\theta_p^{x,y}) \cdot N\left(\frac{2 \cdot d_p^{x,y}}{v \cdot F_s}, \frac{P}{v \cdot F_s}\right) \tag{3}$$

where N is the normal function sampled at a sample rate of F_s in samples per second, v is the velocity in meters per second, and P is the Cartesian grid spacing (0.00159 m for this effort). The normal function is chosen to handle the situation where $d_p^{x,y}$ corresponds to a time between digitized samples.

The scalar $a_p^{x,y}(\theta_p^{x,y})$ is defined based on the beam divergence of the sensor as

$$a_p^{x,y}(\theta_p^{x,y}) = \left(\text{sinc}\left(\frac{D - \sin(\theta_p^{x,y} - \hat{\theta})}{\lambda} \right) \right)^2, \tag{4}$$

where D is the aperture size (0.0254 m for this effort), $\hat{\theta}$ is the radiation angle for this frequency, and λ is the acoustic wavelength. One implication of this relationship is that increasing the aperture size D reduces the beam divergence; since SAFT requires beam overlap between neighboring data acquisition locations for best results; this implies a smaller probe can be better. This functional relationship is based on the intensity pattern created from a plane wave intersecting with a narrow slit; it was found qualitatively to be a reasonable fit to the experimental data. Modeling and/or additional experimentation should be performed to further refine this beam divergence relationship.

The SAFT process is used to combine all the waveforms generated at a single frequency. The result is multiple color map images whose information must be combined to create a single "metaimage" of the weld condition. The process for combining the images used here was to define the metaimage pixel value as the maximum value computed across all images. Algorithmically, this is given as

$$\hat{A}^{x,y} = \max\left(A_1^{x,y}, A_2^{x,y}, ..., A_M^{x,y} \right), \tag{5}$$

where $A_i^{x,y}$ is the SAFT output at location (x,y) at test frequency i and M is the total number of images generated. The justification for using this maximum value approach is that different frequencies are more sensitive to different portions of the weld; taking the maximum value from all SAFT images ensures that a flaw in a difficult to inspect area (i.e., only detectible at a single inspection frequency) is not hidden because the other inspection frequencies do not have sensitivity in that region.

MOCKUP TEST RESULTS

The mockup was evaluated using the transducer and data collection procedure described above. The transducer was connected to a Ritec Inc. SNAP system, which is a hardware system suitable for working with EMAT-type sensors. The SNAP system has a high power (5 kilowatt) gated amplifier that delivers high power radio frequency (RF) tone burst pulses, and is easily customized to meet specific frequency and power requirements. A secondary digital oscilloscope digitized the amplified received signal.

Following data collection using the transducer and SNAP system, SAFT images were generated using the algorithm described above, with one important deviation. It was determined during testing that the SNAP system allowed some energy to leak directly from the transmitter to the receiver RF coil. This leakage produced a ringing in the acquired data from acoustic waves being generated in the receiver PPM array. To overcome this ringing, prior to processing using SAFT, the data collected at the furthest position from the weld was subtracted from all of the other waveforms; in other words, a "baselining" strategy was employed to remove the ringing. The SAFT images that were generated are shown in Fig. 5.

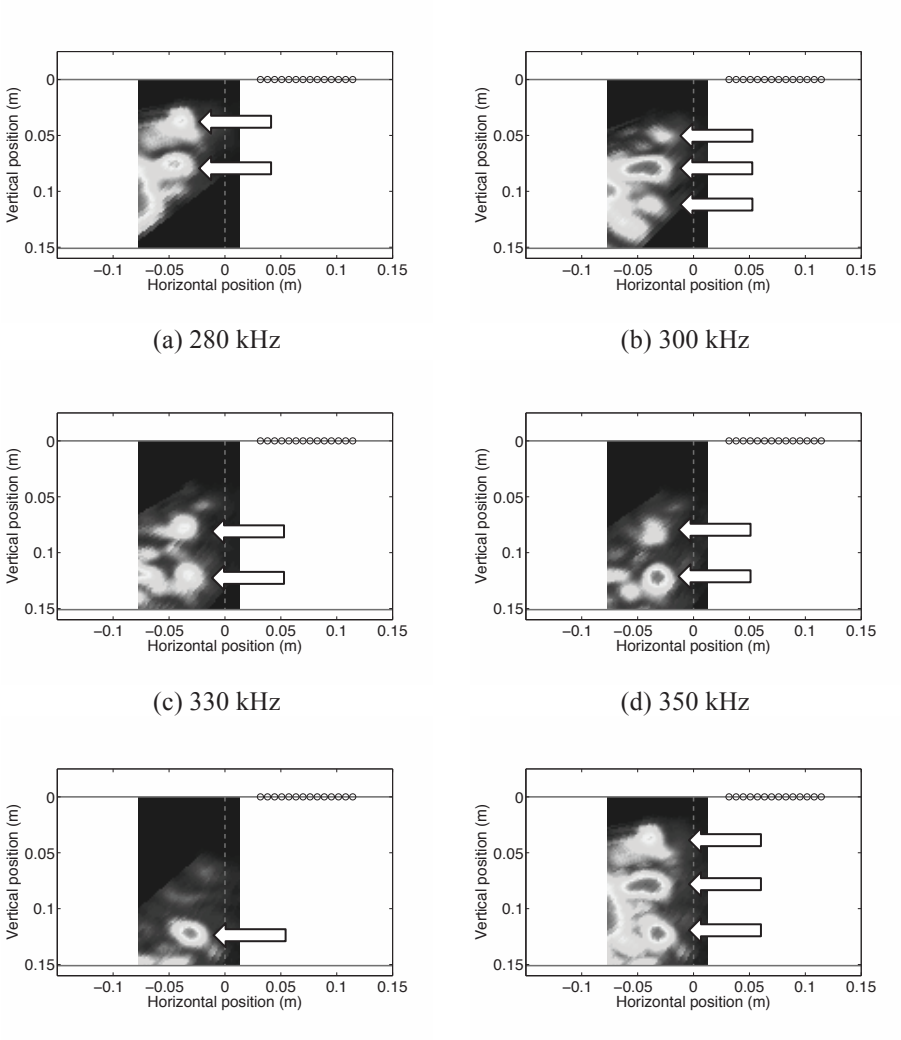

(a) 280 kHz (b) 300 kHz

(c) 330 kHz (d) 350 kHz

(e) 390 kHz (f) Metaimage

FIGURE 5. SAFT imaging results for the five different test frequencies (items (a) through (e)) as well as the metaimage (f) generated from combining the images. The arrows indicate location of flaws in each image, the dashed line represents the front edge of the transducer at start, and the circles show the measurement locations.

Examining the SAFT images, it is clear that each of the defects can be seen, but only one frequency (300 kHz) was able to show all defects simultaneously. The performance as a function of frequency is as would be expected; lower frequencies, with high associated radiation angles, are best at detecting defects near the top surface whereas higher frequencies, with low associated radiation angles, are best at detecting defects near the opposite surface. Moreover, the amplitudes of the nominally identical holes are inconsistent across the different images. Finally, images generated from the lower inspection frequencies' data show a large spurious arrival beyond the flaws. The cause is likely a reflection from the lifting-eye installed in the specimen, some other boundary effect, or sound bouncing between the side-drilled holes. When examining the metaimage, it is clear that this combination image shows all three hole responses simultaneously. Moreover, the amplitude variations between the different hole responses are less dramatic. Unfortunately, the spurious arrival previously observed is also present in the image.

CONCLUSIONS

Overall, the result of the evaluation of the EMAT and inspection procedure was positive; the approach was demonstrated at detecting side-drilled holes located in the center of a DM weld. Moreover, the hardware requirements (transducer and electronics) were less specialized than those required for more conventional phased array approaches previously applied to DM weld inspection. Additionally, the physical size of the EMAT was smaller than many of those used in prior studies while operating at considerably lower test frequencies [7]. Based on these achievements, it can be concluded that the EMAT-based approach for scanning a DM weld by varying the frequency is feasible for inspection of PWR DM weld structures. Moreover, this inspection approach should be applicable to other DM weld structures beyond the problem addressed during this research effort.

To transition the inspection concept from the completed feasibility study to a field-deployable inspection system, several key development efforts must be undertaken (in no particular order of importance):

- Develop algorithms and assess the performance of a 3D SAFT processing for flaws in the DM weld, when circumferential and axial scanning is used.
- Manufacture a mechanized scanner for positioning the EMAT around the DM weld.
- Acquire field-deployable electronics for generating and receiving SH waves using the EMAT at the frequencies of interest and without cross talk between transmit and receive elements.
- Modify ultrasonic data acquisition software to be suitable for waveform acquisition in a field environment.

ACKNOWLEDGMENTS

The presented work benefitted from the input of Dr. Charles Duffer and Mr. Gary Burkhardt, both of whom provided valuable insights regarding the development of the transducer.

REFERENCES

1. H. Gao and B. Lopez, “Development of Single-Channel and Phased Array EMATs for Austenitic Weld Inspection,” Materials Evaluation (ME), Vol. **68** (7), 821-827 (2010)
2. K. Sakamoto, T. Furukawa, I. Komura, Y. Kamiyama, and T. Mihara, “Study on the Ultrasound Propagation in Cast Austenitic Stainless Steel,” Journal of Advanced Maintenance, Vol. **4** (1), 5-25 (2012)
3. United States Nuclear Regulatory Commission, 11555 Rockville Pike, Rockville, MD 20852, http://www.nrc.gov/reactors/operating/ops-experience/pressure-boundary-integrity/weld-issues/index.html
4. Edelmann, X. et al, *Handbook on the Ultrasonic Examination of Austenitic and Dissimilar Welds,* prepared by the Working Group Ultrasonic Testing of Austenitic Welds of the Sub commission VC - Ultrasonically Based Weld Inspection Topics of Commission V of the International Institute of Welding (IIW), First Edition, 1986
5. W. Duetsch and S. Kierspel, K., “Manual Weld Inspection with Ultrasound – Conventionally or with Phased Arrays?,” in *World Conference on Nondestructive Testing-2012 Conference Proceedings*, (2012)
6. Zetec, 8226 Bracken Place SE, Suite 100, Snoqualmie, WA 98065, http://www.zetec.com/products/by-application/piping-weld-inspections/dissimilar-metal-welds (accessed June 2014)
7. United States Nuclear Regulatory Commission, “An Evaluation of Ultrasonic Phased Array Testing for Cast Austenitic Stainless Steel Pressurizer Surge Line Piping Welds,” NUREG/CR-7122, PNNL-19497, Washington, D.C.
8. M. Hirao and H. Ogi, *EMATs for Science and Industry – Noncontacting Ultrasonic Measurements* (Kluwer Academic Publishers, Dordrecht, the Netherlands, 2003)
9. H. Gao, S. Ali, and B. Lopez, “Austenitic Weld Inspection with EMAT Phased Array, http://www.innerspec.com/sites/default/files/Austenitic%20Weld%20Inspection%20with%20EMAT%20Phased%20Array.pdf (accessed June 2014)
10. A. Cobb and J. Fisher, "Nuclear Containment Inspection Using an Array of Guided Wave Sensors for Damage Localization," in *Review of Progress in Quantitative Nondestructive Evaluation*, edited by D. Thompson and D. Chimenti, (American Institute of Physics, Melville, NY, 2010), Vol. 29B, pp. 1713–1720.
11. A. Cobb, C. Duffer, and G. Light, "Evaluation of the Feasibility for Detecting Hidden Corrosion Damage in Multi-layer Gusset Plates using Multiple Inspection Techniques." in *Review of Progress in Quantitative Nondestructive Evaluation*, edited by D. Chimenti, J. Bond and D. Thompson, (American Institute of Physics, Melville, NY, 2014), Vol. 33A, pp. 872–879.